A LETTERS JOURNAL EXPLORING THE FRONTIERS OF PHYSICS

Società Italiana di Fisica

sciences IOP Institute of Physics

The ferromagnetic transition and domain structure in $LiHoF_4$

To cite this article: A. Biltmo and P. Henelius 2009 *EPL* **87** 27007

View the article online for updates and enhancements.

You may also like

- Spectroscopic signatures of the Mott transition on the anisotropic triangular lattice
Rajarshi Tiwari and Pinaki Majumdar
- Impact of CNT medium on the interaction between ferromagnetic nanoparticles
A. L. Danilyuk, I. V. Komissarov, A. V. Kukharev et al.
- The effects of non-linear electron-phonon interactions on superconductivity and charge-density-wave correlations
Shaozhi Li and S. Johnston

This content was downloaded from IP address 18.119.126.80 on 20/04/2024 at 07:14

epl A Letters Journal Exploring the Frontiers of Physics

July 2009

EPL, **87** (2009) 27007
doi: 10.1209/0295-5075/87/27007

www.epljournal.org

The ferromagnetic transition and domain structure in $LiHoF_4$

A. Biltmo and P. Henelius[(a)]

Department of Theoretical Physics, Royal Institute of Technology - SE-106 91 Stockholm, Sweden, EU

received 17 March 2009; accepted in final form 7 July 2009
published online 4 August 2009

PACS 75.10.Hk – Classical spin models
PACS 75.40.Mg – Numerical simulation studies
PACS 75.50.Dd – Nonmetallic ferromagnetic materials

Abstract – Using Monte Carlo simulations we verify that the rare-earth compound $LiHoF_4$ is a very good realization of a dipolar Ising model. With only one free parameter our calculations for the magnetization, specific heat and inverse susceptibility match experimental data at a quantitative level in the 0.5–3 kelvin range, including the ferromagnetic transition at 1.53 K. Using parallel tempering methods and reaching system sizes up to 32000 dipoles with periodic boundary conditions, we are able to give evidence of the logarithmic corrections predicted in renormalization group theory. Due to the long range and angular dependence of the dipolar model, sample shape and domains play a crucial role in the ordered state. We consider surface corrections to Griffiths's theorem, which arise in finite macroscopic samples and lead to a theory of magnetic domains. We find a domain wall energy of $0.059\,\mathrm{erg/cm^2}$ and predict that the ground-state domain structure for cylinders with a demagnetization factor $N > 0$ consists of thin parallel sheets of opposite magnetization, with a width depending on the demagnetization factor.

Copyright © EPLA, 2009

Introduction. – The use of effective theories is one of the primary *modus operandi* of modern physics. Frequently, the effective models give only a qualitatively accurate description of the phenomena under investigation, due to corrections that are omitted and free parameters that may be hard to determine experimentally. Finding experimental systems that display striking phenomena, are accurately described by a simple model, and have few or no free parameters, is important since it enables detailed comparison between experiments, theory and numerical simulations.

The rare-earth magnet $LiHo_xY_{1-x}F_4$ displays an array of fascinating magnetic phenomena such as quantum phase transitions [1], spin-glass behavior [2] and persistent coherent oscillations [3]. Yet the pure material $LiHoF_4$ is believed to be described by one of the most fundamental models in condensed-matter physics: the two-state Ising model. Materials such as the antiferromagnets $DyPO_4$ and $Dy_3Al_5O_{12}$ have been shown to be accurately described by a *short-range* Ising model [4]. In $LiHoF_4$, on the other hand, the magnetic properties are dominated by the *long-range* dipolar interaction. Since the interaction strength is set by the known g factor it is possible to determine the effective model to high accuracy. However, the inherent frustration and long range of the dipolar model make direct numerical simulations demanding. Using a parallel tempering Monte Carlo (MC) method that is essentially free of systematic errors (apart from finite-size effects) we go beyond mean-field theory and explicitly demonstrate that the experimental data for $LiHoF_4$ is indeed in quantitative agreement with the dipolar Ising model.

The effective model. – The magnetic properties of $LiHoF_4$ originate in the $4f$-electrons of the Ho^{3+} ions, which sit in a tetragonal lattice with a unit cell of size (1,1,2.077) in units of $a = 5.175\,\text{Å}$. According to Hund's rules, the holmium ion has a ${}^5I_8$ ground state, but the crystal field partially lifts the 17-fold degeneracy, and the resulting doubly degenerate ground state is separated from the first excited state by 11 K [5]. This separation of energy levels enables a projection of the full Hamiltonian onto the ground-state subspace [6]. The matrix elements of the operators J^x and J^y vanish in this subspace, and the effective model is the dipolar Ising model

$$H = \frac{J_d}{2} \sum_{i,j} \frac{r_{ij}^2 - 3z_{ij}^2}{r_{ij}^5} \sigma_i^z \sigma_j^z + J_e \sum_{\langle ij \rangle} \sigma_i^z \sigma_j^z. \qquad (1)$$

The dipolar coupling constant is given by $J_d = (g\mu_B/2)^2/a^3 = 0.214\,\mathrm{K}$ due to the renormalized g factor $\simeq 13.8$, which can be computed from the crystal-field

[(a)] E-mail: henelius@kth.se

Hamiltonian [6], or deduced from the experimental high-temperature susceptibility [7]. The only free parameter in the model, the weak exchange interaction, has no fundamental physical effect on the system other than to alter the critical temperature (T_c). We set it to $J_e = 0.12\,\mathrm{K}$ to reduce the T_c of the model from 1.91 K to the experimental value 1.53 K [6,8,9].

The study of the dipolar interaction has a long and interesting history. Demagnetization effects, whereby the surface charge of a magnetized body causes a self-field, are important. For ellipsoidal samples the field is given by $\mathbf{H} = -N\mathbf{M}$, where N is the shape-dependent demagnetization factor and $\mathbf{M}$ is the magnetization [10]. Due to demagnetization effects, Luttinger and Tisza found a ground-state energy that depends on both lattice structure and sample shape [11]. Griffiths later gave a proof that the free energy, without applied fields, is independent of sample shape [12]. The apparent contradiction is explained in terms of domain formation, allowing the magnetic order to vary from one macroscopic part of the system to the next. Experimentally this has been demonstrated since measurements of the specific heat for $LiHoF_4$ show no apparent shape dependence [13], and needle-shaped domains have been observed close to the transition [14].

The dipolar interaction has several properties that complicate a numerical treatment of the model. Inherent frustration combined with the long range makes MC equilibration cumbersome at low temperatures, requiring long simulation runs to reach equilibrium. To handle the long range of the interactions we employ the method of Ewald summation [15]. This method not only gives improved numerical convergence due to the use of periodic boundary conditions, but also includes a parameter which emulates different sample shapes [16–18]. Our simulations have been carried out using single-flip parallel tempering MC, since cluster methods are of limited use in frustrated systems. The MC sample is of size L^3 unit cells, with four spins per unit cell, and the linear size L ranging from 10 to 20 (4000 to 32000 spins) throughout the study. In most figures we use about 100 temperature points resulting in smooth curves.

Thermodynamic properties. – In order to investigate the convergence to the thermodynamic limit we first consider the effect of different sample shapes on the internal energy in fig. 1. The calculation is performed for a long needle (with demagnetization factor $N = 0$) and for a sphere ($N = 4\pi/3$). The energy for the needle converges quickly in system size and we show the converged curve. The energy for the sphere coincides with the energy for the needle above T_c, but shows large finite-size corrections below T_c. The needle orders ferromagnetically, and according to Griffiths's theorem the infinite spherical sample must have the same energy. If the spherical sample forms ferromagnetic domains that cancel the internal magnetic field, then the two energies will be equal. The formation of domains can be seen directly in the simulations of the spherical sample, and in fig. 2 we show a typical spin configuration at $T = 0.5\,T_c$. Note that the domain configuration breaks the symmetry of the Monte Carlo cell, and the domain walls spontaneously align along the x or y axes. In the inset of fig. 1 we see that the difference of the two energies decreases as the inverse of the volume of the system. Similar results were observed in a study of a dipolar liquid, where the inclusion of a finite demagnetization factor caused domain formation [19,20].

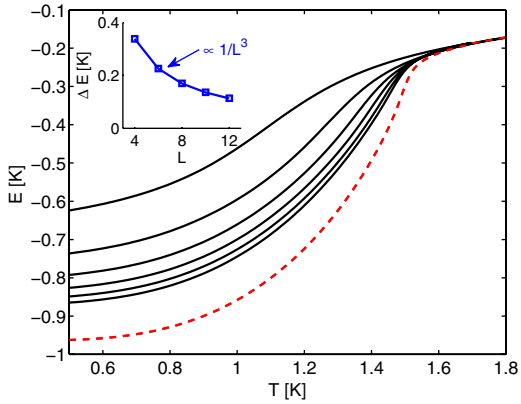

Fig. 1: (Colour on-line) The internal energy for spherical ($N = 4\pi/3$, black lines) and needle-shaped ($N = 0$, dashed red line) boundary conditions. For the spherical boundary the MC cell is of size L^3 unit cells with $L = 4$, 6, 8, 10, 12 and 14 from top to bottom. The inset shows the difference of the two energies as a function of system size at $T = 0.5\,\mathrm{K}$.

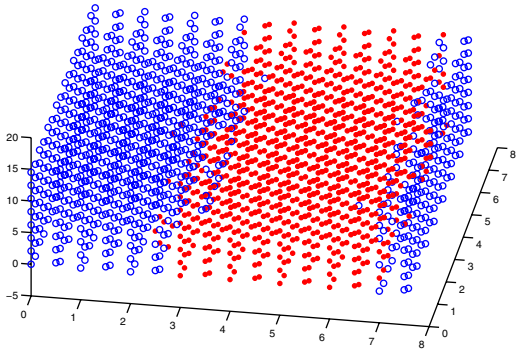

Fig. 2: (Colour on-line) Typical spin configuration for spherical boundary conditions at $T = 0.5\,T_c$. Open and filled symbols indicate different Ising spin states and two domains with separating domain walls are clearly visible.

In order to verify the accuracy of our effective model for $LiHoF_4$ we make detailed comparisons between our calculations and existing experimental data. In fig. 3 we show the specific-heat measurements from refs. [13,21], and our calculations for spherical ($N = 4\pi/3$) and needle-shaped ($N = 0$) samples. Again we find that the numerical results for spherical samples show slow convergence, while the results for zero demagnetization factor have converged, except for close to the critical temperature where

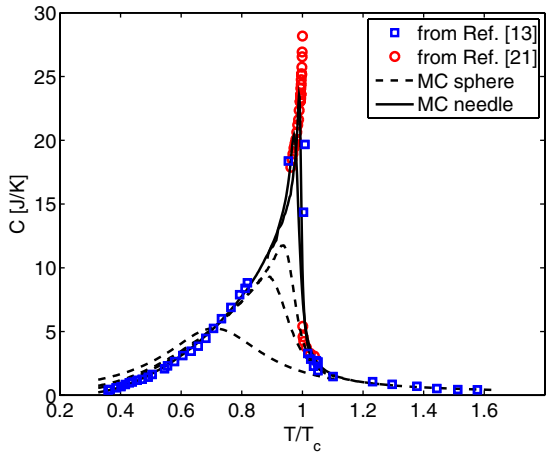

Fig. 3: (Colour on-line) The specific-heat capacity for spherical ($N = 4\pi/3$; $L = 12$, 10 and 8 from top to bottom) and needle-shaped boundary conditions ($N = 0$; $L = 20$ and 18 from top to bottom), and experimental data for a spherical sample [13] as well as an oblate sample [21,22].

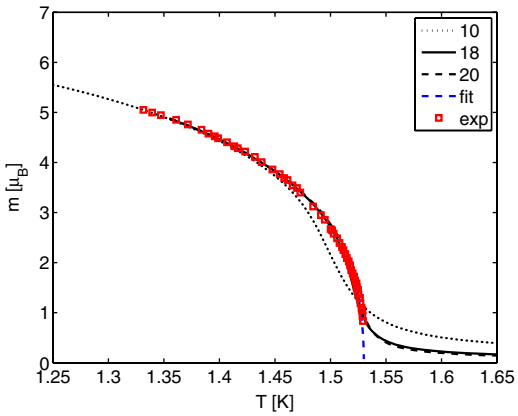

Fig. 4: (Colour on-line) Magnetization as a function of temperature for system sizes $L = 10$, 18 and 20, as well as experimental data [22]. Close to the critical temperature we show a fit to our data including logarithmic corrections.

finite-size effects are still visible. In the range of converged data the numerical results agree very well with the experimental data.

Next, we compare the spontaneous intradomain magnetization measured by Griffin *et al.* [22] with our simulations for zero demagnetization factor in fig. 4. The experimental data is only determined up to a constant, and we have normalized the experimental data to agree with our calculations at 1.35 K. The agreement is very good all the way up to about $0.96\,T_c$, where finite-size effects become visible in our largest system sizes. Below we will analyze our data more carefully and demonstrate that we can directly observe logarithmic corrections to the mean-field magnetization.

In addition to the magnetization and specific-heat data there is also experimental data available for the

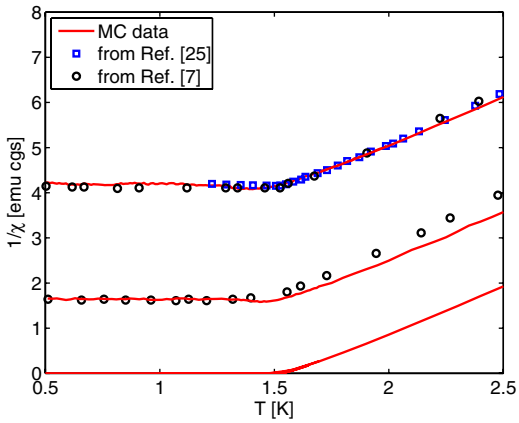

Fig. 5: (Colour on-line) The inverse magnetic susceptibility $1/\chi$ from experiments and simulations. The three sets of curves correspond to $N = 4\pi/3$ (spherical sample), 1.65 and 0 from top to bottom.

susceptibility. Here we consider the inverse magnetic susceptibility as measured by Cooke *et al.* [7] as a function of different demagnetization factors. We compare our calculations to the measurements of a spherical sample and a long cylinder, for which the demagnetization factors were determined to $N = 4.15$ and $N = 1.65$ [7]. In fig. 5 we demonstrate that the agreement with experiments again is very good for $N = 4\pi/3$ (spherical sample) and $N = 1.65$. The interesting behavior of the inverse susceptibility below T_c can be understood in terms of the domains [7]. With no disorder the walls are free to move and arrange themselves to cancel the internal field: $\mathbf{H}_{int} = \mathbf{H} - N\mathbf{M} = 0$, resulting in a constant susceptibility, $\chi = \mathbf{M}/\mathbf{H} = 1/N$, below T_c. We find it remarkable that the numerical simulations for limited system sizes have converged so well, even if the domain size is much smaller than in the real material. Above T_c the Curie-Weiss law is followed. For the $N = 1.65$ sample we note that the initial slope of the experimental data is slightly higher than the MC data, a fact that could be due to non-stoichiometry in the material used by Cooke *et al.* [7].

The upper critical dimension is three for uniaxial dipolar interactions [23], and according to renormalization group theory, the magnetization, susceptibility and specific heat are predicted to have logarithmic corrections of the form $\log|(T - T_c)/T_0|^{1/3}$, where T_0 is an effective temperature. Experimentally, logarithmic corrections have been convincingly seen in the magnetization [22] of $LiHoF_4$ and the specific heat of $LiTbF_4$ [24], but not in the susceptibility [25].

Numerical studies of the dipolar model have applied finite-size scaling to detect the logarithmic corrections [26,27] and in one study [26] the authors conclude that the collapse was enhanced when logarithmic corrections were added to the standard scaling form, but at the expense of using different critical temperatures with and without logarithmic corrections. Another study applies a different

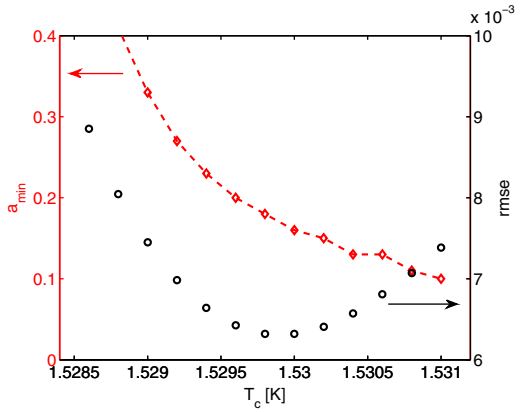

Fig. 6: (Colour on-line) Exponent a of the logarithmic corrections and rmse for the optimal fit of the magnetization curve as a function of T_c.

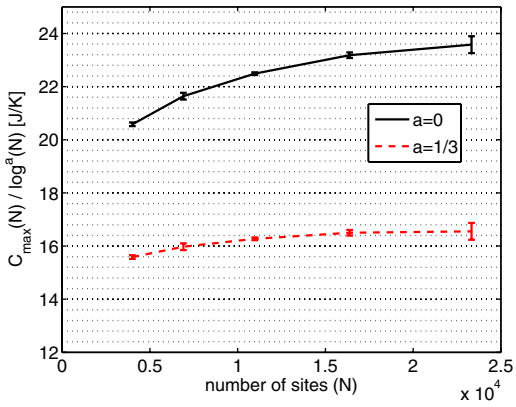

Fig. 7: (Colour on-line) The peak of the heat capacity grows logarithmically with system size.

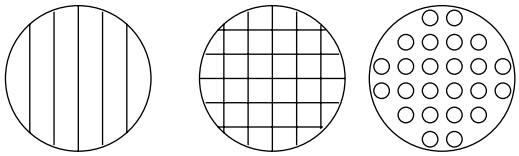

Fig. 8: Domain configurations of parallel sheets (E_2), a checkerboard pattern (E_4) and cylinders (E_c).

scaling form [27], which uses more free parameters to include standard corrections to scaling, and also shows an improved collapse of the data. We have applied the above finite-size scaling to our data, and find that if we include standard corrections to scaling, as well a logarithmic corrections, then the collapse is very good both with and without logarithmic corrections, making it hard to verify the logarithmic corrections.

Since we have results for large system sizes (32000 spins) we instead attempt to directly fit a curve of the form

$$m(T) \sim (T - T_c)^{1/2} |\log |(T - T_c)/T_0||^a \qquad (2)$$

to the part of the critical region where the MC data has converged. For different values of T_c we let T_0 and the exponent a vary, and display the value of a that gives the best fit, together with the corresponding root mean squared error (rmse) in fig. 6. There is a minimum in the rmse around $a = 0.18$, giving numerical evidence of non-zero logarithmic corrections. However, the exact value of the optimal T_c and a depends on the temperature interval included in the fit, but a finite value of a does improve the fit.

For the thermodynamic quantities that diverge at the critical point we have not been able to use the same direct fit due to the large finite-size effects. However, convincing evidence for logarithmic corrections in the heat capacity can still be obtained by plotting the peak height against a logarithmically corrected system size. This curve should tend to a constant for large system sizes, and as can be seen in fig. 7 the curve levels out significantly faster for the predicted exponent $a = 1/3$ [23] than for the mean-field result $a = 0$.

Magnetic domains. – Griffiths's theorem predicts the formation of domains in order to make the free energy independent of sample shape, but it does not answer the fundamental question of the size and shape of the domains. The domain structure is the result of an energy balance between bulk and surface contributions [28]. In the absence of a demagnetization field the ground state for the dipolar model we consider is ferromagnetic, and the introduction of a domain wall increases the bulk dipolar energy by an amount proportional to the area of the domain wall. However, the magnetostatic energy is given by a surface integral over the magnetic surface charge density, and this energy decreases linearly with the size of the domains. Considering a cylinder with the magnetization direction along the axis, the total energy per unit surface area (top and bottom) is [28]

$$E = \delta\mu M^2 D + \alpha L\sigma/D, \qquad (3)$$

where D is the linear size of the domain, L the length of the cylinder, σ the domain wall energy density, and the prefactors δ and α are determined by the geometric domain wall configuration. The energy is minimized by a domain width $D = \sqrt{\frac{\alpha L\sigma}{\delta\mu M^2}}$ which results in an energy $E = 2\sqrt{\delta\alpha\mu M^2 L\sigma}$.

A previous theoretical study of domain formation in general Ising dipolar magnets focused on the striped structure, and in particular on the so-called branching, where spikes of opposite magnetization form near the surface of the sample [29,30]. Domain walls in $LiHoF_4$ have been theoretically studied in the context of a possible roughening transition [31], but here our goal is to calculate the ground-state domain structure, energy and size using material specific parameters for $LiHoF_4$. We consider three domain structures [28] that may be relevant for $LiHoF_4$: thin parallel sheets (E_2, with $\delta = 1.7$, $\alpha = 1$), checkerboard (E_4, with $\delta = 1.06$, $\alpha = 2$) and cylinders (E_c, with $\delta = 0.74$,

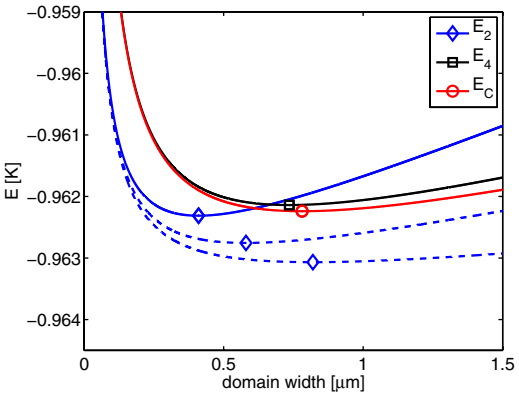

Fig. 9: (Colour on-line) The energy per spin for parallel sheets (E_2), checkerboard (E_4) and cylindrical (E_c) domain structures for a cylinder of diameter 3.2 mm and height 4.8 mm (solid curves). Dashed curves show E_2 for cylinders of increasing heights 9.6 mm and 19.2 mm.

$\alpha = \sqrt{2\pi}$), depicted in fig. 8. Since the total energy is proportional to $\sqrt{\delta\sigma}$, which is lowest for E_2, we expect the ground-state configuration to consist of parallel sheets. However, in order to calculate the size of the domains we need to know the domain wall energy density, σ, which we consider next.

Using the Ewald summation technique we can compute the total energy of the *infinite* periodic domain configuration E_2 as a function of domain width. Since the domain structure has zero total magnetic surface charge, the magnetostatic surface term becomes negligible in the limit of infinite system size, and the energy is of the form $E = \alpha L\sigma/D + E^0$, where we have explicitly included the ground-state energy E^0. We note that this is the bulk limit considered by Griffiths, and as the domain size grows the ground-state energy for $LiHoF_4$ always approaches the energy of the ferromagnetic ground state for zero demagnetization factor, in accordance with Griffiths's theorem. We carried out computations up to linear domain sizes of 30 unit cells. Since finite-size effects are very small the total energy follows the form $E = C_1/D + C_2$ to very high accuracy already for very small domain sizes, allowing us to extract the constants C_1 and C_2. For the periodic stripe pattern our calculation yields $E = (0.598/D - 0.9638)\,\mathrm{K/spin}$, where D is the linear dimension of the stripe in units of 5.175 Å, and $-0.9638\,\mathrm{K/spin}$ is the ferromagnetic-ground-state energy. From the first term (0.5898 K/spin) we find the domain wall energy $\sigma = 0.059\,\mathrm{erg/cm^2}$ for $LiHoF_4$. This can be compared to typical domain wall energies in iron of about $1\,\mathrm{erg/cm^2}$ [28].

Having calculated the domain wall energy, we plot the energy per spin as a function of domain size in the fully polarized ground state for the three configurations in fig. 9. As expected, the configuration of parallel sheets has the lowest energy. The calculation was done for a cylinder of diameter 3.2 mm and length 4.8 mm [14]. We also show E_2 for lengths 9.6 mm and 19.2 mm. As the ratio of end surface to bulk decreases, the demagnetization factor of the cylinder decreases and the size of the domains grows, as shown in fig. 9. As the cylinder grows longer we also see that the total energy approaches the ferromagnetic-ground-state energy $-0.9638\,\mathrm{K/spin}$. From fig. 9 we consequently see that for finite samples there is a small shape dependence of the energy, which disappears in the limit of infinite system size considered by Griffiths.

We are aware of two experimental observations of the domain structure in $LiHoF_4$. In ref. [14] needle-shaped domains of size $5\,\mu$m at $T = 0.92\,T_c$ were observed in a cylinder appropriate for our calculation, but unfortunately no measurements were reported close to the ground state. A different set of measurements were made at slightly lower temperature ($T = 0.87\,T_c$) in a slab-like geometry of thickness 0.67 mm [32]. In zero applied field a stripe-like structure appears with a width of about $3\,\mu$m. However, the inhomogeneity of the demagnetization field causes branching near the surface of the crystal, an effect which we have not considered here. Furthermore, the pure stripe pattern is also broken up by dislocations and fluctuations [32]. It would therefore be very interesting to experimentally observe the ground-state domain structure at a lower temperature in a clean crystal, to see whether the theory presented here suffices to determine the ground-state domain structure.

Conclusion and summary. – We have provided strong evidence that the rare-earth magnet $LiHoF_4$ is a very good realization of the dipolar Ising model. This enables detailed comparisons of theory, experiments and simulations. As examples of this we give evidence of the logarithmic corrections predicted by renormalization group theory for the dipolar model, and we predict that the ground-state domain configuration for cylindrically shaped samples consists of thin parallel sheets. $LiHoF_4$ is an excellent testing ground for theories of domains because the domain walls have no width, very clean single crystals are available, and domains appear naturally in MC simulations. In particular, we believe there is much further scope for the study of domain wall motion in the presence of disorder and transverse fields.

* * *

This work was supported by the Göran Gustafsson foundation and the Swedish Research Council.

REFERENCES

[1] Bitko D., Rosenbaum T. F. and Aeppli G., *Phys. Rev. Lett.*, **77** (1996) 940.
[2] Reich D. H., Ellman B., Yang J., Rosenbaum T. F., Aeppli G. and Belanger D. P., *Phys. Rev. B*, **42** (1990) 4631.
[3] Ghosh S., Parthasarathy R., Rosenbaum T. F. and Aeppli G., *Science*, **296** (2002) 2195.
[4] Wolf W. P., *Braz. J. Phys.*, **30** (2000) 794.

[5] Hansen P. E., Johansson T. and Nevald R., *Phys. Rev. B*, **12** (1975) 5315.
[6] Chakraborty P. B., Henelius P., Kjønsberg H., Sandvik A. W. and Girvin S. M., *Phys. Rev. B*, **70** (2004) 144411.
[7] Cooke A. H., Jones D. A., Silva J. F. A. and Wells M. R., *J. Phys. C*, **8** (1975) 4083.
[8] Biltmo A. and Henelius P., *Phys. Rev. B*, **76** (2007) 054423.
[9] Tabei S. M. A., Gingras M. J. P., Kao Y. J. and Yavors'kii T., *Phys. Rev. B*, **78** (2008) 184408.
[10] Jackson J. D., *Classical Electromagnetism* (J. Wiley) 1998.
[11] Luttinger J. M. and Tisza L., *Phys. Rev.*, **70** (1946) 954.
[12] Griffiths R., *Phys. Rev.*, **176** (1968) 655.
[13] Mennenga G., de Jongh L. J. and Huiskamp W. J., *J. Magn. & Magn. Mater.*, **44** (1984) 59.
[14] Battison J. E., Kasten A., Leask M. J. M., Lowry J. B. and Wanklyn B. M., *J. Phys. C*, **8** (1975) 4089.
[15] Ewald P. P., *Ann. Phys. (Leipzig)*, **369** (1921) 253.
[16] de Leeuw S. W., Perram J. W. and Smith E. R., *Annu. Rev. Phys. Chem.*, **37** (1990) 245.
[17] Melko R. G. and Gingras M. J. P., *J. Phys.: Condens. Matter*, **16** (2004) R1277.
[18] Groh B. and Dietrich S., *Phys. Rev. E*, **63** (2000) 021203.
[19] Wei D. and Patey G. N., *Phys. Rev. Lett.*, **68** (1992) 2043.
[20] Wei D. and Patey G. N., *Phys. Rev. A*, **46** (1992) 7783.
[21] Nikkel J. and Ellman B., *Phys. Rev. B*, **64** (2001) 214420.
[22] Griffin J. A., Huster M. and Folweiler R. J., *Phys. Rev. B*, **22** (1980) 4370.
[23] Larkin A. I. and Khmel'nitskij D. E., *Sov. Phys. JETP*, **29** (1969) 1123.
[24] Ahlers G., Kornblit A. and Guggenheim H., *Phys. Rev. Lett.*, **34** (1975) 1227.
[25] Beauvillain P., Renard J. P., Laursen I. and Walker P. J., *Phys. Rev. B*, **18** (1978) 3360.
[26] Xu H.-J., Bergersen B. and Racz Z., *J. Phys.: Condens. Matter*, **4** (1992) 2035.
[27] Klopper A. V., Rössler U. K. and Stamps R. L., *Eur. Phys. J. B*, **50** (2006) 45.
[28] Kittel C., *Rev. Mod. Phys.*, **21** (1949) 541.
[29] Gabay M. and Garel T., *Phys.* (*Paris*), *Lett.*, **45** (1984) 989.
[30] Gabay M. and Garel T., *Phys.* (*Paris*), **46** (1985) 5.
[31] Mias G. I. and Girvin S. M., *Phys. Rev. B*, **72** (2005) 064411.
[32] Meyer P., Pommer J. and Ferre J., in *Electro-optic and Magneto-optic Materials and Applications, Proc. SPIE*, **1126** (1989) 93.